Geochemistry Geophysics Geosystems G3
AN ELECTRONIC JOURNAL OF THE EARTH SCIENCES
Published by AGU and the Geochemical Society

Article
Volume 7, Number 4
12 April 2006
Q04P11, doi:10.1029/2005GC000984
ISSN: 1525-2027

Pleistocene variability of the Subtropical Convergence at East Tasman Plateau: Evidence from planktonic foraminiferal Mg/Ca (ODP Site 1172A)

Dirk Nürnberg and Jeroen Groeneveld

Leibniz-Institut für Meereswissenschaften (IFM-GEOMAR), Wischhofstr. 1–3, D-24148 Kiel, Germany (dnuernberg@ifm-geomar.de)

[1] Combined measurements of Mg/Ca and stable oxygen isotopes in tests of the planktonic foraminifer *G. bulloides* from Ocean Drilling Program (ODP) Site 1172A (East Tasman Plateau) allowed us to reconstruct sea surface temperature ($SST_{Mg/Ca}$), sea surface salinity (SSS), and hence variations in the Subtropical Convergence (STC) in the southwestern Tasman Sea over the last four major glacial-interglacial changes. During interglacials the commonly enhanced $SST_{Mg/Ca}$ and SSS correspond to a lowered marine productivity and a lowered terrigenous flux, implying that the STC separating cool, high-nutrient Subantarctic Surface Water from warm, saline, oligotrophic Subtropical Surface Water and hence the band of zonal westerlies responsible for the eolian dust flux were located south of East Tasman Plateau. The warm East Australian Current was well established during warm periods and propagated far south. During glacial times, $SST_{Mg/Ca}$ and SSS were lower, while both marine productivity and eolian flux increased. Such conditions prevailed during glacial Marine Isotope Stages MIS 12, MIS 10, and to a lesser degree MIS 6 and implied the extended northward influence of Subantarctic Surface Water and a shift of the STC to <44°S. The overall climatic signal at Site 1172A appears to be largely attenuated when compared to published climate records from comparable latitudes to the west and to the east. $SST_{Mg/Ca}$ amplitudes were more pronounced in the subantarctic Indian Ocean and at Chatham Rise. They exhibit a consistent pattern suggesting that latitudinal shifts of the STC occurred synchronously in the subantarctic Indian Ocean and at Chatham Rise but were largely damped at East Tasman Plateau due to the influence of the East Australian Current.

Components: 10,842 words, 9 figures.

Keywords: Mg/Ca paleothermometry; paleosalinity; planktonic foraminifera.

Index Terms: 3344 Atmospheric Processes: Paleoclimatology (0473, 4900); 3030 Marine Geology and Geophysics: Micropaleontology (0459, 4944); 9330 Geographic Location: Australia; 9604 Information Related to Geologic Time: Cenozoic.

Received 30 March 2005; **Revised** 21 October 2005; **Accepted** 16 December 2005; **Published** 12 April 2006.

Nürnberg, D., and J. Groeneveld (2006), Pleistocene variability of the Subtropical Convergence at East Tasman Plateau: Evidence from planktonic foraminiferal Mg/Ca (ODP Site 1172A), *Geochem. Geophys. Geosyst.*, *7*, Q04P11, doi:10.1029/2005GC000984.

Theme: Development of the Foraminiferal Mg/Ca Proxy for Paleoceanography
Guest Editor: Pamela Martin

1. Introduction

[2] Previous paleoceanographic and paleoclimatic reconstructions based on sediment sequences from the South Tasman region showed that the Tasmanian Seaway was a region of high oceanographic complexity closely linked to global ocean and climate dynamics [e.g., *Kennett*, 1977]. Today,

the ocean east of Tasmania is characterized by the seasonally changing influence of oligotrophic, subtropical, and high salinity surface water masses of the East Australian Current, which originates in the Coral Sea and flows southward along the east Australian coast. Strength and nature of this western boundary current are controlled mainly by the West Pacific Warm Pool, where much heat and moisture is transferred from the ocean to the atmosphere. In direct response, the Subtropical Convergence (STC) separating subantarctic and subtropical surface waters latitudinally varies and affects considerably the distribution pattern of sea surface temperature, primary productivity, and moisture supply along southeastern Australia [*Garner*, 1959; *Tchernia*, 1980; *Cresswell*, 1987; *Villanoy and Tomczak*, 1991].

[3] Changes in ocean surface hydrography west and east of Australia on long glacial/interglacial time scales were described previously [e.g., *Williams*, 1976; *Morley*, 1989; *Almond et al.*, 1993; *François et al.*, 1993; *Okada and Wells*, 1997; *Passlow et al.*, 1997; *Nees et al.*, 1999; *Nürnberg et al.*, 2004]. Northward propagations of the Subtropical Convergence occurred through much of the Quaternary, while poleward movements of the front were reported only during the Holocene and at interglacial marine oxygen isotope stages (MIS) 5.5, 9, and 11 [*Kershaw et al.*, 2000]. In the Indian Ocean, spatial variations of the STC and the Polar Front were described by *Hays et al.* [1976], *Prell et al.* [1979, 1986], *Howard and Prell* [1992], and *Armand* [1997]. Northward movements of the Polar Front were described by *Morley and Hays* [1979] and *Nürnberg et al.* [1997] for the southern South Atlantic Ocean. In response to frontal migration, sea surface temperatures changed accordingly as inferred from various techniques [*Morley et al.*, 1988; *Morley*, 1989; *Labracherie et al.*, 1989; *Howard and Prell*, 1992; *Pichon et al.*, 1992], and specifically within the STC marine productivity peaked during glacial times [e.g., *Howard and Prell*, 1992]. It is still debated, however, whether or not the changes in frontal positions took place synchronously or time-transgressively [*Morley*, 1989; *Howard and Prell*, 1992].

[4] Our study, based on sediment material from Ocean Drilling Program (ODP) Site 1172A recovered during Leg 189 from East Tasman Plateau, focuses on the spatial and temporal reconstruction of the surface ocean hydrography in the southwestern Tasman Sea during the last ~500,000 years, and relates these changes to both the Pleistocene Southern Ocean and the global dynamic paleoceanographic and paleoclimatic evolution. In particular, we applied the combined approach of Mg/Ca-paleothermometry and stable oxygen isotope geochemistry on planktonic foraminifers in order to (1) define and quantify climatically induced sea surface temperature (SST) and salinity (SSS) changes on orbital timescales, (2) relate SST changes to variations in marine productivity and terrigenous flux, (3) reveal the glacial/interglacial interplay between variations in the East Australian Current system and the STC, (4) relate the southwestern Tasman Sea variability in SST and SSS to other mid-southern latitude records from the southern Indian Ocean and Chatham Rise, and (5) relate temporal changes in the oceanographic patterns of the study area to glacial/interglacial variations in the strength of the West Pacific Warm Pool, and to the Antarctic climate record.

[5] The study area is mainly affected by the STC, a key component of the sensitive, climatically relevant Southern Ocean [*Howard and Prell*, 1992], where warm, saline Subtropical Surface Water is in contact with the less saline Subantarctic Surface Water [*Martinez*, 1994a]. The STC, considered to be the northern extent of the Southern Ocean, varies seasonally and zonally. The core of the modern STC is located at ~45°S in the Tasman Sea [*Edwards and Emery*, 1982; *Belkin and Gordon*, 1996; *Rintoul et al.*, 1997], and hence exhibits a significant displacement to the south in the Australian sector [*Orsi et al.*, 1995]. The STC is recognized by the surface pattern of isotherms and the close spacing of isohalines [*Villanoy and Tomczak*, 1991]. It closely follows the 15°C surface summer isotherm, the 10°C winter isotherm, and the 34.7–34.8 salinity isopleth [*Garner*, 1959]. Meanders and eddies are an integral structural feature of the frontal system [*Tchernia*, 1980; *Cresswell*, 1987]. Mixing of these water masses induces high seasonal phytoplankton productivity, and a nutrient gradient from subtropical to subantarctic waters. For paleoceanographic reconstructions, the front is commonly identified by a sea surface temperature gradient of ~4°C across 1° latitude [*Sikes et al.*, 2002].

[6] The prominent surface current in the study area is the East Australian Current. The swift and narrow East Australian Current is highly variable and complex, and ferries up to 30 Sv of high temperature (20–26°C) and low salinity waters (35.4–35.6) from the equatorial region into the

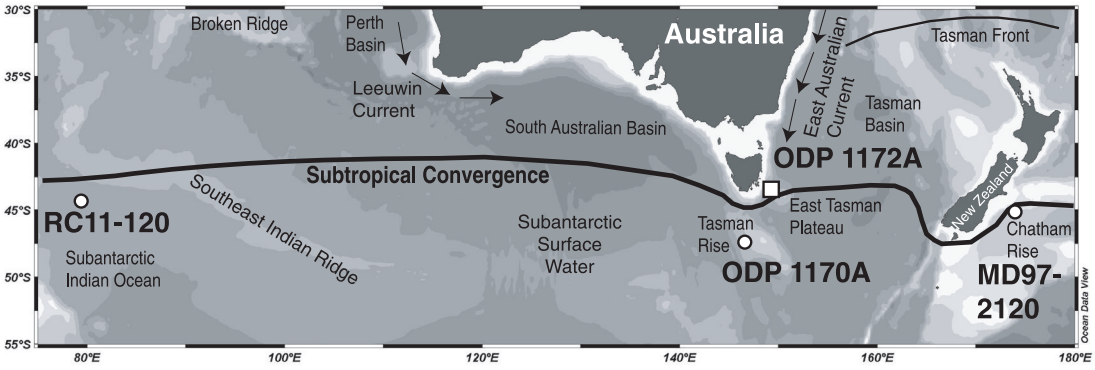

Figure 1. Bathymetry of the Australian sector of the Southern Ocean showing the location of ODP Site 1172A (open square) at East Tasman Plateau. Core locations of interest to this study are also indicated (open circles). All sites lie at comparable southern latitudes close to the Subtropical Convergence (black line). Most prominent surface currents around Australia are included.

Tasman Sea, sometimes as far as 42°S near Bass Strait. South of ~32°S, large warm core anticyclonic eddies of Coral Sea water are the dominant feature of the EAC affecting the thermal structure down to 1300 m water depth. The perennial current is strongest between December and April. Along the seafloor beneath the EAC there is a compensating northward flowing undercurrent. Near Tasmania, the meandering East Australian Current becomes unstable, and pinches off to form energetic eddies once or twice a year.

2. Material and Methods

2.1. Sediment Material

[7] We present a Mg/Ca-paleotemperature record ($SST_{Mg/Ca}$) from Site 1172A drilled during ODP Leg 189 at East Tasman Plateau (43°57.585′S 149°55.696′E) (Figure 1). It is located at 2621.9 m water depth, and is bathed by Circumpolar Deep Water. The largely continuous Neogene sediment sequence is dominated by pelagic foraminiferal nannofossil oozes. Supplementary data on marine productivity and terrigenous flux were presented elsewhere [*Nürnberg et al.*, 2004], but will be used for comparison.

[8] Calcite dissolution clearly alters the foraminiferal Mg/Ca ratios [e.g., *Dekens et al.*, 2002]. Hence knowledge on the present position of the carbonate lysocline and its depth variation through time is essential for the interpretation of the Mg/Ca signal. *Martinez* [1994b] reconstructed the modern lysocline level in the western Tasman Basin using fragmentation ratios of planktonic foraminifers and suggested that the lysocline depth is at ~3600 m, which is ~1000 m below the Site 1172A location. On the basis of downcore variations of the foraminiferal fragmentation ratio at Tasman Plateau (core E36-23, 2521 m water depth), *Martinez* [1994b] concluded that the lysocline markedly shallowed only during Marine Isotope Stages (MIS) 8 and 11. *Sturm* [2004] added that the lysocline depth fluctuated between >4100 m (glacial) and <3200 m (interglacial) in the Australian sector of the Southern Ocean during the last 500 kyr, thus remaining several hundred meters below the Site 1172A location. The lysocline appears to be shallower than in the South Atlantic and equatorial Pacific, which is possibly due to the inflow of older, recirculated, and more CO_2-enriched deep-water masses from the Pacific and Indian Oceans into the Circumpolar Deep Water and Antarctic Bottom Water masses [*Sturm*, 2004].

2.2. Chronostratigraphy

[9] The Late Pleistocene chronostratigraphy of Site 1172A was first presented by *Nürnberg et al.* [2004]. It is initially based on the graphic correlation of prominent maxima and minima in the benthic oxygen isotope curve with the reference oxygen isotope record of *Shackleton et al.* [1990], ODP Site 677 (Figure 2). The correlation was performed with AnalySeries Version 1.1 [*Paillard et al.*, 1996]. In order to further refine the chronostratigraphy of Site 1172A, the reflectivity record of Site 1172A was tied to that of Site 1170A

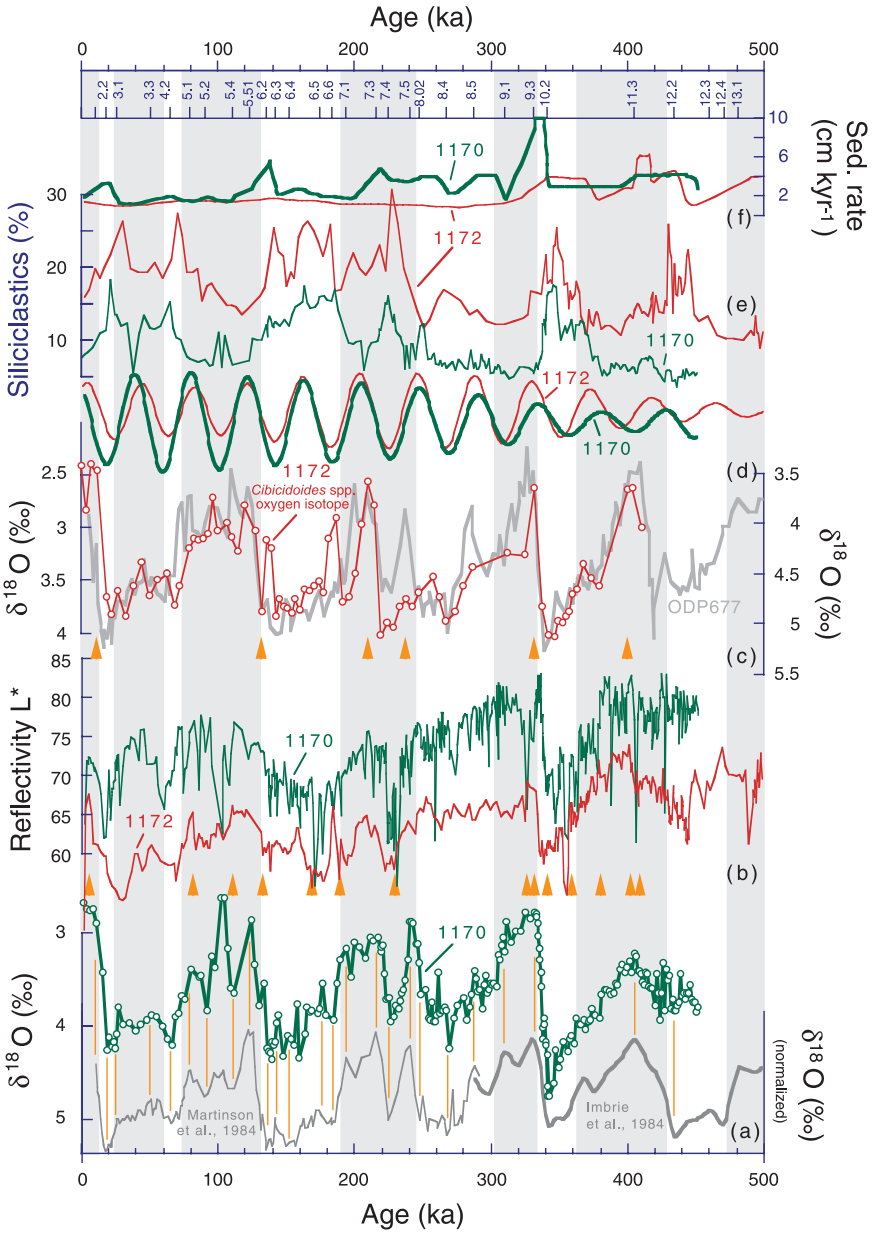

Figure 2. Stratigraphical framework of Site 1172A based on the graphic correlation with Site 1170A from South Tasman Rise. The age model of Site 1170A [*Nürnberg et al.*, 2004] was established by (a) correlating the benthic oxygen isotope record (green line with circles, left scale) younger than Marine Oxygen Isotope event 8.5 to the stacked reference curve of *Martinson et al.* [1987]. The SPECMAP Stack [*Imbrie et al.*, 1984] was used from event 8.5 to 13.2 (tie points are indicated by thin vertical lines). The age model for Site 1172A is based both (b) on the graphic correlation of the reflectivity record of Site 1172A with that of Site 1170A (arrows indicate tie points) and (c) on the correlation of prominent maxima and minima in the benthic oxygen isotope record of Site 1172A (red line with circles, left scale, arrows indicate tie points) with the ODP Site 677 $\delta^{18}O$ reference record of *Shackleton et al.* (thick gray line, right scale). The resemblance of both (d) the filtered 41-kyr components of the reflectivity records and (e) typical structures of the siliciclastic records of Sites 1172A and 1170A allowed the detailed correlation of both sediment records and thus a transfer of age control points. The percentages of siliciclastic (terrigenous) material were calculated by subtracting % $CaCO_3$ and % TOC (total organic carbon) from bulk sediment [*Nürnberg et al.*, 2004]. (f) Sedimentation rates are generally low and vary between ~1 cm kyr^{-1} and ~4 cm kyr^{-1}. Shaded areas indicate odd marine oxygen isotope stages.

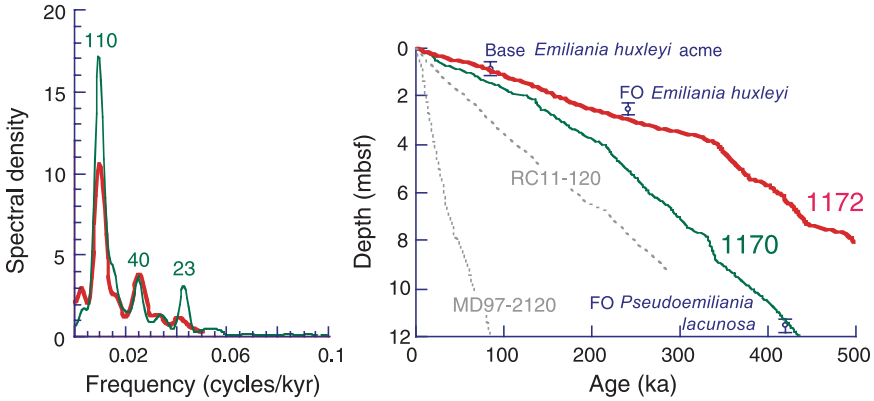

Figure 3. (left) Frequency spectra for the benthic oxygen isotope data of Sites 1172A and 1170A displaying dominant cyclicities of ~100 kyr, 41 kyr, and 23 kyr as a response to cyclic fluctuations in the Earth's orbital parameters eccentricity, obliquity, and precession. The recognition of these cyclicities corroborates the accuracy of the age models. (right) According depth versus age diagrams. The Site 1170 biostratographic events Base *Emiliania huxleyi* acme at 84,000 ka (0.855 mbsf ± 0.25 m), FO *Emiliania huxleyi* at 240,000 ka (2.555 mbsf ± 0.25 m), and LO Pseudoemiliania lacunosa at 420,000 ka (11.55 mbsf ± 0.25 m) [*Stickley et al.*, 2004] are indicated. Cores of interest to this study are stippled.

(Figure 2). The chronostratigraphy of Site 1170A from South Tasman Rise [*Nürnberg et al.*, 2004], which exhibits a better temporal resolution, was established by correlating the benthic oxygen isotope record younger than Marine Isotope (MIS) event 8.5 to the stacked reference curve of *Martinson et al.* [1987]. The SPECMAP Stack [*Imbrie et al.*, 1984] was used from MIS events 8.5 to 13.2. The marine oxygen isotope stages were recognized using the standard nomenclature proposed by *Prell et al.* [1986] and *Tiedemann et al.* [1994]. Ages and stratigraphic levels of paleomagnetic reversals [*Exon et al.*, 2001] were used as a basis for initial correlation at Site 1170A. A few biostratigraphical datums within the Late Quaternary time period of Site 1170A [*Stickley et al.*, 2004] were also considered, although these datums deviate from our benthic oxygen isotope-based age model, presumably due to the insufficient sampling density for biostratigraphy (Figure 3). The frequency spectra of the oxygen isotope data of Sites 1170A and 1172A display dominant cyclicities of ~100 kyr, ~41 kyr, and ~23 kyr as a response to cyclic fluctuations in the Earth's orbital parameters eccentricity, obliquity, and precession (Figure 3). The recognition of these cyclicities corroborates the accuracy of the Site 1170A and 1172A age models. Sedimentation rates are generally low and vary between ~1 cm kyr^{-1} and ~4 cm kyr^{-1}, only occasionally increasing to maximum 10 cm kyr^{-1} during short time intervals (Figure 2). The commonly low sedimentation rates during the last 500 kyr are comparable with estimates of *Nees et al.* [1999] for an adjacent core site on South Tasman Rise. They are lower than those of cores RC11-120 and MD97-2120, the Mg/Ca and stable oxygen isotope records of which are used for comparison (Figure 3). Both the low sedimentation rates and the low-resolution sampling at Site 1172A may have contributed to a muted amplitude in the paleorecords.

2.3. Analysis of Foraminiferal Mg/Ca and Stable Oxygen Isotopes

[10] Sea surface temperatures (SST) were calculated from foraminiferal Mg/Ca ratios [*Nürnberg*, 2000]. On the basis of previous experience, the Mg/Ca-paleothermometry has an accuracy of ±0.5–1°C [e.g., *Mashiotta et al.*, 1999; *Lea et al.*, 2000; *Nürnberg et al.*, 2000]. Most advantageous to other SST-proxies, Mg/Ca is measured on the same biotic carrier as stable oxygen isotopes ($\delta^{18}O$), thereby avoiding the bias of seasonality and/or habitat differences that occur when proxy data from different faunal groups are used.

[11] The planktonic foraminifer *Globigerina bulloides* was selected for Mg/Ca analyses. It is a typical transitional to subpolar species, tolerating a wide temperature range with optimum temperatures between 10°C and 20°C [*Niebler*, 1995; *Wang et al.*, 1995]. The spinose, non-symbiotic species preferentially inhabits shallow waters (~50 m water depth) [*Hemleben et al.*, 1989], although *Berger* [1989] described specimens in plankton nets from >150 m. *Giraudeau* [1993] postulated that the distribution and abundance pattern of the heterotroph [*Hemleben and Spindler*,

1983] *G. bulloides* is often driven by nutrient supply. Most recently, *King and Howard* [2003] revealed from sediment trap and core top studies from the Subtropical and Subantarctic Zones south of Tasmania that the observed foraminiferal austral spring flux is dominated by *G. bulloides*. The maximum flux in *G. bulloides* is further associated with a deepening of the mixed layer depth and the concurrent increase in chlorophyll-a concentrations [*King and Howard*, 2003]. At South Chatham Rise, peak fluxes of *G. bulloides* are restricted to austral spring (September, October) [*King and Howard*, 2003].

[12] Specimens of *G. bulloides* were selected from the 250–500 μm size fraction. With a few exceptions, sample spacing was 5 cm between 0.03 and 8.13 mbsf, covering the last ~500 ka. Foraminiferal tests visibly contaminated by ferromanganese oxides were discarded. Mg/Ca analyses were performed after intense cleaning of foraminiferal tests. The cleaning protocol was adopted from *Barker et al.* [2003]. Approximately 0.5–1.2 mg sample material, usually consisting of ~40–50 specimens of *G. bulloide*s, was gently crushed between glass plates to open the chambers, and subsequently placed into vials previously cleaned with 10% HNO_3 (p.a.). To remove contaminant phases, the material was rinsed 4–6 times with distilled deionized water with ultrasonical cleaning (2 min) after each rinse. Two methanol (suprapure) washes alternated with ultrasonic cleaning and, again, one distilled deionized water rinse followed. Samples were then treated with a hot (~100°C) oxidizing 1% $NaOH/H_2O_2$ solution (10 mL 0.1 *N* NaOH (analytical grade); 100 μL 30% H_2O_2 (suprapure)) for 10 min. Every 2.5 min, the vials were rapped on the bench top to release any gaseous buildup. After 5 min, samples were placed in an ultrasonic bath for a few seconds to maintain contact between reagent and sample. This treatment was repeated after refreshment of the oxidizing solution. The oxidizing solution was removed in three rinses with distilled deionized water. The clean foraminiferal fragments were placed in clean vials, and 250 μL of 0.001 *M* HNO_3 (subboiled distilled) was added. Ultrasonic treatment for 30 seconds, and two rinses with distilled deionized water followed removal of the HNO_3. After removal of any remaining solution, the samples were dissolved in 500 μL of 0.075 *M* HNO_3 (subboiled distilled) during ultrasonic treatment. The sample solution was then diluted to 3 mL with distilled deionized water containing 10 ppm of yttrium as an internal standard.

[13] Analyses were run on an ICP-AES (ISA Jobin Yvon-Spex Instruments S.A. GmbH) with polychromator. We selected element lines for analyses that appeared most intense and undisturbed (Ca: 317.93 nm; Mg: 279.55 nm; Mn: 257.61 nm; Fe: 238.21 nm; Y: 371.03 nm). Element detection was performed with photomultipliers, the high tension of which was adapted to each element concentration range. Every analysis consists of a triplet of repetitive measurements. The relative standard deviation of all measurements performed is ~0.93% for magnesium, and 0.12% for calcium. Mg/Ca reproducibility of a few replicate samples of *G. bulloides* provides a mean standard deviation of 0.04 mmol/mol for Mg/Ca. The conversion of foraminiferal Mg/Ca ratios into $SST_{Mg/Ca}$ was accomplished according to the algorithm of *Mashiotta et al.* [1999]: $Mg/Ca = 0.474\ e^{0.107\ SST}$, $R^2 = 0.98$. The error in terms of $SST_{Mg/Ca}$ is ±0.8°C. The calibration of *Mashiotta et al.* [1999] is based on Mg/Ca from cultured and Subantarctic Southern Ocean core-top foraminifers related to laboratory and sea surface temperatures. At temperatures <17°C, it is equivalent to the *Elderfield and Ganssen* [2000] calibration, which related foraminiferal Mg/Ca to subsurface foraminiferal calcification depths. For Site 1172A, the difference in $SST_{Mg/Ca}$ between both calibrations is 0.2°C on average. To identify contaminant clay particles and manganese-rich carbonate coatings, which might affect the foraminiferal Mg/Ca ratios [*Boyle*, 1983, *Barker et al.*, 2003], iron and manganese concentrations were monitored. The manganese and iron concentrations were commonly below the detection limit of 1.2 ppb (0.02 mmol) and 8 ppb (0.14 mmol), respectively, of our analytical device. Taking into account a mean calcium concentration of 44 ppm (1.1 mol), resulting Mn/Ca ratios and Fe/Ca ratios were <0.02 mmol/mol and <0.13 mmol/mol, respectively. Hence Mn/Ca and Fe/Ca ratios are even below the 0.1 mmol/mol Mn/Ca and Fe/Ca ratios given by *Barker et al.* [2003] for clean, uncontaminated foraminiferal tests.

[14] In addition, we performed $\delta^{18}O$ analyses on 10 specimens/sample of the planktonic foraminifer *G. bulloides*. These specimens originate from the same samples and size fractions as specimens that were measured for Mg/Ca. The tests were ultrasonically cleaned in distilled deionized water prior to analyses. The isotopic analyses of the planktonic foraminifers were performed with a Finnigan MAT 252 mass spectrometer equipped with an automated Kiel Carbonate Preparation line. The mass spectrometer is calibrated to NBS 19, and the

isotope values are reported on the VPDB (Vienna PDB) scale. The external reproducibility of in-house carbonate standards was ±0.08‰ for $\delta^{18}O$ and 0.04‰ for $\delta^{13}C$ (1 σ values). All results are reported in ‰ relative to VPDB. All analytical data presented are available electronically through the Wold Data Center-A for Paleoclimatology, NOAA/NGDC, 325 Broadway, Boulder, CO 80303, USA (http://www.ngdc.noaa.gov/paleo; email: paleo@mail.ngdc.noaa.gov). Leg 189 shipboard data are available at the ODP Janus Database (http://www-odp.tamu.edu/database/).

2.4. Calculation of $\delta^{18}O_{seawater}$ and Assessment of Paleo-Sea Surface Salinities (SSS)

[15] The calculation of $\delta^{18}O_{seawater}$ and paleo-SSS follows *Pahnke et al.* [2003] in order to stay compatible with other records from the Southern Ocean [*Mashiotta et al.*, 1999; *Pahnke et al.*, 2003]. First, to calculate $\delta^{18}O_{seawater}$ the paleotemperature equation of *Shackleton* [1974] was applied:

$$\delta^{18}O_{seawater} = \delta^{18}O_{foram} + 0.27 - ((4.38 - \sqrt{(4.382 - 4 * 0.1 * (16.9. - SST_{Mg/Ca}))})/(2 * 0.1)) \quad (1)$$

This equation implies that the oxygen isotope fractionation between $CaCO_3$ and water basically increases by about 0.25‰ for each degree the water is cooled [*Epstein et al.*, 1953; *Shackleton*, 1974]. 0.27 is the *Hut* [1987]offset to convert from calcite on the Pee Dee Belemnite scale (PDB) to water on the Standard Mean Ocean Water scale (SMOW). Prior to calculation of $\delta^{18}O_{seawater}$, the $\delta^{18}O_{foram}$ was corrected for the global ice volume signal. Although there are different approaches to assess ice volume changes through time [e.g., *Labeyrie et al.*, 1987; *Shackleton*, 1987; *Vogelsang*, 1990; *Wang et al.*, 1995; *Jouzel et al.*, 2002; *Siddall et al.*, 2003], we applied the *Waelbroeck et al.* [2002] mean-ocean $\delta^{18}O_{seawater}$ record as a reasonable approximation for variations in the global ice volume. It is based on benthic oxygen isotope records from various ocean areas and covers the last four climatic cycles. In particular for the last 20 ka, the *Waelbroeck et al.* [2002] mean-ocean $\delta^{18}O_{seawater}$ record closely follows the records of sea level change of *Fairbanks* [1989], *Bard et al.* [1996], *Okuno and Nakada* [1999], *Guilderson et al.* [2000], and *Hanebuth et al.* [2000]. As the record is correlated to the *Martinson et al.* [1987] $\delta^{18}O$ reference stack, it is congruent with our Site 1172A age model, and also applied by *Pahnke et al.* [2003] for paleosalinity reconstructions at Chatham Rise.

[16] The local $\delta^{18}O_{seawater}$ anomaly, as derived from $\delta^{18}O_{foram}$ and $SST_{Mg/Ca}$ after correcting $\delta^{18}O_{foram}$ for mean ocean $\delta^{18}O_{seawater}$ changes, was then calculated using the mean late Holocene (0–6 kyr) value as a reference. $\delta^{18}O_{seawater}$ was converted into the equivalent salinity record by using a regional $\delta^{18}O_{seawater}$-salinity relationship, which is based on surface ocean data from 40°S–50°S (G. A. Schmidt et al., http://www.giss.nasa.gov/data/o18data/, 1999): SSS = 1.465 $\delta^{18}O_{seawater}$ + 34.00 (r^2 = 0.81 [see *Pahnke et al.*, 2003]). The local salinity anomaly is again calculated using the mean late Holocene (0–6 kyr) value as a reference. The application of a modern linear $^{18}O_{seawater}$-salinity relationship is not really warranted, because of temporal nonlinearities in the $^{18}O_{seawater}$-salinity relationship. These nonlinearities arise from changing evaporation, freshwater input, and the impact of sea ice [*Rohling and Bigg*, 1998; *Roche et al.*, 2004]. Apart from these temporal effects, spatial variability of the freshwater budget and sea ice effects cause regionally dependant $^{18}O_{seawater}$-salinity relationships [*Rohling and Bigg*, 1998]. The local freshwater budget, comprising evaporation/precipitation processes, and river discharge, is considered of minor importance for the East Tasman Plateau area. Fluvial freshwater contribution today and even during glacial times is of subordinate importance. In eastern and central Australia, riverine activity was dramatically reduced during glacial times [e.g., *Nanson et al.*, 1992] as aridity increased with vegetation becoming more open and grasslands expanding across much of the continent [*Harle*, 1997]. Extensive summer sea ice melting might have affected large parts of the high-latitude ocean [*CLIMAP*, 1981]. But the effect on the East Tasman Plateau area remains unclear, although *Pahnke et al.* [2003] suspected that the low-$\delta^{18}O$ meltwater from Antarctica and disintegrating New Zealand glaciers might have altered the modern Southern Ocean $^{18}O_{seawater}$-salinity relationship. Finally, advection of water masses is considered most important for determining regional $^{18}O_{seawater}$-salinity relationships, exceeding the influence of the local freshwater balance [*Rohling and Bigg*, 1998]. In fact, the two water masses separated by the STC reveal differences in their modern S:$\delta^{18}O$ ratio. According to the G. A. Schmidt et al. (http://www.giss.nasa.gov/data/o18data/, 1999) database, subtropical surface waters (80–180°E and 140–180°W, 40–30°S, 0–50 m water depth) exhibit a S:$\delta^{18}O$ ratio of

1:0.34, whereas subantarctic surface waters (80–180°E, 55–45°S, 0–50 m water depth) have a S:$\delta^{18}O$ ratio of 1:0.53 close to the ratio of 0.50 in the Pacific and in the Atlantic oceans [*Broecker*, 1989]. Hence mixing of water masses along the STC and changing influence at the Site 1172A core location through time might have effectively changed the $^{18}O_{seawater}$-salinity relationship.

[17] On the basis of the uncertainties in calculating the local $\delta^{18}O_{seawater}$ and the unwarranted assumption of a linear $^{18}O_{seawater}$-salinity relationship being constant over time, *Rohling* [2000] provided theoretical minimum error bars of ±0.3 to 0.7 to the paleosalinity estimates, rarely falling below ±0.6 for most reconstructions. By using a modern $^{18}O_{seawater}$-salinity relationship, *Pahnke et al.* [2003] noted that their amplitudes of salinity changes at Chatham Rise might have been overestimated, but that their overall pattern of paleosalinities was not affected.

3. Results and Discussion

3.1. Core-Top Foraminiferal $SST_{Mg/Ca}$ in Comparison to Modern Conditions

[18] As the modern carbonate lysocline is ~1000 m below the present depth of Site 1172A (~2600 m), carbonate dissolution affecting foraminiferal Mg/Ca is assumed to be of less importance. Nevertheless, the variability in Mg/Ca (1.47–1.66 mmol/mol, mean: ~1.56 mmol/mol), and hence in $SST_{Mg/Ca}$ (~10.6–11.7°C, mean: ~11.2°C), is relatively high in the uppermost ~80 cm of Site 1172A (<~6 ka). In order to test the correctness and reliability of the $SST_{Mg/Ca}$ reconstructions, and to further support current assumptions on the habitat depth of *G. bulloides* and the time of Mg/Ca-signal formation at East Tasman Plateau, we related the average late Holocene (<6 ka) $SST_{Mg/Ca}$ of ~11.2°C to modern ocean temperatures. Figure 4 presents temperature profiles at East Tasman Plateau [*Levitus and Boyer*, 1994] showing large seasonal differences. The reconstructed late Holocene $SST_{Mg/Ca}$ of ~11.2°C is much closer to the modern austral spring water temperature of ~11.5–12°C at 50–100 m water depth (the presumed depth habitat of *G. bulloides*) than to the summer/autumn temperature of ~13.5–15°C, suggesting that *G. bulloides* from Site 1172A records austral spring temperature conditions at that depth interval. This is congruent to the Subantarctic sediment trap studies of *King and Howard* [2003], who found the highest flux of *G. bulloides* during austral spring, when the mixed layer deepens. The slightly too low $SST_{Mg/Ca}$ estimate of ~11.2°C might be explained by inconsistencies in the applied calibration curve. In fact, the Mg/Ca ratios of South Atlantic core-top foraminifers from below ~4 km water depth used in the *Mashiotta et al.* [1999] Mg/Ca versus temperature calibration might have been perturbed by calcite dissolution, leading to a too steep run of the calibration curve.

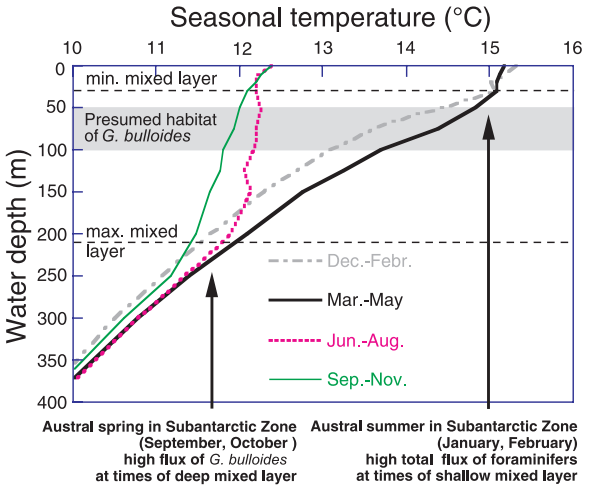

Figure 4. Seasonal temperature profiles at East Tasman Plateau from *Levitus and Boyer* [1994]. During austral spring (September to November), the mixed layer in the Subantarctic Zone is thick (thin line), while during summer (December to February), the mixed layer is considerably shallower (thick hatched line). According to *King and Howard* [2003], the highest flux of *G. bulloides* occurs during austral spring, when the mixed layer deepens. At that time, the monthly water temperature range is ~11.5–12°C at ~50–100 m water depth, the presumed habitat of *G. bulloides* [*Levitus and Boyer*, 1994]. The reconstructed late Holocene (<~6 ka) $SST_{Mg/Ca}$ of ~11.2°C is closer to the modern austral spring water temperature than to the summer/autumn temperature of ~13.5–15°C, suggesting that *G. bulloides* from Site 1172A records austral spring temperature conditions at 50–100 m water depth.

3.2. Pleistocene Variability of $SST_{Mg/Ca}$ Over East Tasman Plateau

[19] The downcore Mg/Ca record of Site 1172A from East Tasman Plateau spans the last ~500,000 years (MIS 1–13), thus comprising four major glacial-interglacial changes. Mg/Ca ratios in *G. bulloides* range between 1.2 and 2.0 mmol/mol (Figure 5). Downcore variations of foraminiferal Mg/Ca ratios follow changes seen in the planktonic and benthic oxygen isotopes, and clearly reflect glacial-interglacial changes. High Mg/Ca ratios

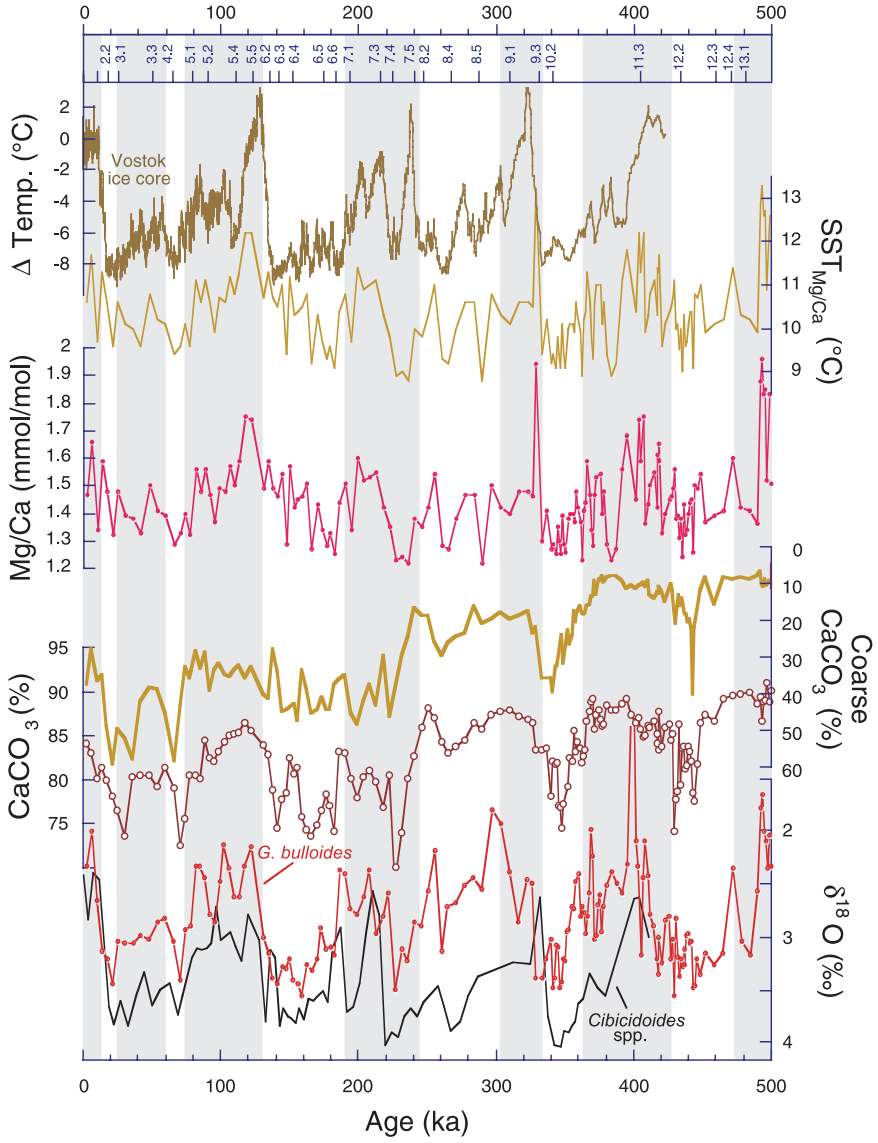

Figure 5. Foraminiferal Mg/Ca data (*G. bulloides*) and the according $SST_{Mg/Ca}$ reconstruction at Site 1172A in comparison to planktonic (red line with dots) and benthic oxygen isotopes (black line) from the same species and samples. Downcore oscillations of foraminiferal Mg/Ca ratios are coherent with oscillations seen in the planktonic oxygen isotopes and clearly reflect glacial-interglacial changes. The $SST_{Mg/Ca}$ scale is based on conversion of Mg/Ca data using the relationship of *Mashiotta et al.* [1999]. For comparison, the Antarctic atmospheric temperature record derived from the deuterium isotope (δD) record of the Vostok ice core is plotted, based on the age scale of *Petit et al.* [1999]. Atmospheric temperatures are presented as deviations from the modern value (ΔTemp.). $CaCO_3$ concentrations are anticorrelated to coarse (>63 μm) carbonate concentrations [*Nürnberg et al.*, 2004], implying good $CaCO_3$ preservation. Shaded areas indicate odd marine oxygen isotope stages.

occur during interglacial MIS 1, 5, 7, 9, 11, and 13, with Mg/Ca maxima during MIS 9 and 13. Low values commonly occur during the glacial periods. This pattern is not congruent with the foraminiferal fragmentation records from deeper core sites at South Tasman Rise (>3000 m water depth), which point to calcite dissolution mainly during MIS 8, 9 and 11 [*Sturm*, 2004]. The apparent anticorrelation between $CaCO_3$ percentages (entirely composed of biogenic components) and the percentages of coarse carbonate (>63 μm) at the shallower Site 1172A, instead, implies that at times of low $CaCO_3$ deposition the contribution of planktonic foraminifers to the bulk $CaCO_3$ increased (Figure 5). We would have expected the opposite (low $CaCO_3$ and low coarse carbonate due to the fragmentation of planktonic foraminiferal tests), if the $CaCO_3$ record would have resulted from calcite dissolution. Hence

we assume that carbonate preservation at Site 1172A is good and that the foraminiferal Mg/Ca signal is unaffected by dissolution.

[20] Sea surface temperatures derived from foraminiferal Mg/Ca provide a maximum temperature range of ~5°C, from 9°C to 14°C. At terminations, the glacial/interglacial amplitude is ~2–3°C. On orbital timescales, the $SST_{Mg/Ca}$ record of ODP Site 1172A follows the Vostok deuterium isotope (δD) record, which reflects air temperatures over Antarctica (Figure 5). The fine structure of the δD record with prominent cooling events like the Antarctic Cold Reversal [*Petit et al.*, 1999; *Blunier and Brook*, 2001] and the mid-Termination III reversal (250–242 ka) [*Petit et al.*, 1999; *Caillon et al.*, 2003], however, is not seen in the low resolution $SST_{Mg/Ca}$ record of Site 1172A. The prominent temperature maximum in Antarctica during MIS 7.5 is not reflected, neither in the $SST_{Mg/Ca}$ record of Site 1172A, nor in the planktonic and benthic $\delta^{18}O$ records. Instead, Site 1172A exhibits a $SST_{Mg/Ca}$ maximum during MIS 13.3, which exceeds all other maxima. The Antarctic air temperature amplitudes across Termination I, II and III of 9.5°C, 12.3°C, and 9.3°C, respectively, are much higher than the $SST_{Mg/Ca}$ amplitudes at East Tasman Plateau (Termination I: ~2°C; Termination II: ~3°C; Termination IV: ~4°C; Termination V: ~2.5°C). Apparently, the East Tasman Plateau surface ocean did not react on the strong atmospheric cooling during glacials in Antarctica, which was most likely caused by the increasing thermal isolation with glacially strengthened circum-Antarctic surface circulation [*Cox*, 1989].

3.3. Pleistocene $SST_{Mg/Ca}$ Variability at East Tasman Plateau in Comparison to the Subantarctic Indian Ocean and Chatham Rise

[21] We compared Site 1172A to two Southern Ocean $SST_{Mg/Ca}$ records from comparable southern latitudes. Core RC11-120 is from the subantarctic Indian Ocean [*Mashiotta et al.*, 1999], and core MD97-2120 was recovered from Chatham Rise [*Pahnke et al.*, 2003]. Both site locations are slightly south of the present-day STC (Figure 1). The warm period $SST_{Mg/Ca}$ at East Tasman Plateau (Site 1172A) are close to the temperature estimates of *Mashiotta et al.* [1999] for the subantarctic Indian Ocean (RC11-120). In contrast, the glacial $SST_{Mg/Ca}$ for the subantarctic Indian Ocean tend to be lower by ~2°C (Figure 6). Hence the glacial/interglacial $SST_{Mg/Ca}$ signal at Site 1172A is clearly attenuated in comparison to the subantarctic Indian Ocean record, which shows glacial/interglacial amplitudes of 3°C, 4°C and 4.5°C at terminations I, II, and III, respectively. The $SST_{Mg/Ca}$ at Chatham Rise (MD97-2120) are consistently higher during interglacial periods than the other $SST_{Mg/Ca}$ records, and glacial/interglacial amplitudes are significantly larger (4.9–6.8°C) [*Pahnke et al.*, 2003]. The last glacial/interglacial $SST_{Mg/Ca}$ amplitude of 4.9°C is within the range of amplitudes of 4°C and 6°C that is derived from alkenones and foraminiferal census counts at nearby core-sites [*Wells and Okada*, 1997; *Sikes et al.*, 2002; *Pahnke et al.*, 2003]. The glacial $SST_{Mg/Ca}$ at Chatham Rise, instead, approach those of Site 1172A.

[22] The planktonic foraminiferal $\delta^{18}O$ pattern looks different (Figure 6). The $\delta^{18}O$ record of subantarctic Indian Ocean core RC11-120 [*Mashiotta et al.*, 1999] is nearly identical to Site 1172A. Both records resemble the smoothed $\delta^{18}O$ record of Chatham Rise core MD97-2120 [*Pahnke et al.*, 2003], the original data of which exhibit a much larger amplitude. The planktonic $\delta^{18}O$ records of both East Tasman Plateau Site 1172A and the subantarctic Indian Ocean core RC11-120 are lighter by ~0.5‰ during glacials, and heavier by ~0.5‰ during interglacials.

3.4. Pleistocene $\delta^{18}O_{seawater}$ and Paleosalinity Variability Over East Tasman Plateau in Comparison to the Subantarctic Indian Ocean and Chatham Rise

[23] How can the observed differences in planktonic $\delta^{18}O_{foram}$ and $SST_{Mg/Ca}$ between Southern Ocean core locations be explained in terms of oceanographic changes? As all sites discussed here are located close to the Subtropical Convergence (STC), which separates warm saline Subtropical Surface Water from less saline, cool Subantarctic Surface Water [*Martinez*, 1994b], changes in SST and SSS across site locations may provide information on spatial and temporal changes of this oceanographic frontal feature. We therefore calculated the $\delta^{18}O_{seawater}$ from the combined use of $\delta^{18}O_{foram}$ and $SST_{Mg/Ca}$ in the paleotemperature equation of *Shackleton* [1974], and subsequently estimated SSS from $\delta^{18}O_{seawater}$.

[24] $\delta^{18}O_{seawater}$ at Site 1172A ranges between –0.2 and +2‰ at most (Figure 7). The resulting SSS record, expressed as deviation from the Holocene (0–6 ka) mean value, shows pronounced and high-amplitude glacial/interglacial changes before

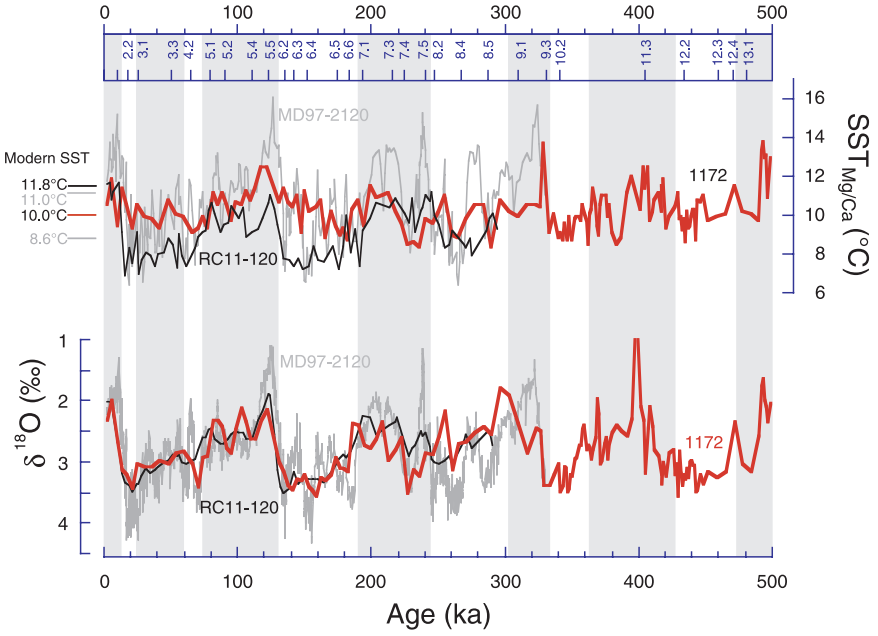

Figure 6. Comparison of $SST_{Mg/Ca}$ and $\delta^{18}O$ records of *G. bulloides* from three Southern Ocean sites from comparable southern latitude. Thick red line: ODP Site 1172A from East Tasman Rise (this study); thin black line: RC11-120 from the subantarctic Indian Ocean [*Mashiotta et al.*, 1999] (43°31′S 79°52′E, 3135 m); thin gray line: MD97-2120 from Chatham Rise [*Pahnke et al.*, 2003] (45°32′S 174°56′E, 1210 m). At Site 1172A, the glacial/interglacial $SST_{Mg/Ca}$ amplitude is ~2–3°C, which appears to be attenuated in comparison to the subantarctic Indian Ocean and the Chatham Rise records. Modern SST estimates (left side) are from September–October and from 50–100 m water depth according to *Levitus and Boyer* [1994]. For core MD97-2120, the discrepancy between modern SST estimates of 8.6°C and 11°C from *Levitus and Boyer* and *Uddstrom and Oien* [1999], respectively, may be explained by different definitions for sea surface temperatures (8.6°C: September–October and from 50–100 m water depth; 11°C: annual temperature at 0 m water depth). Shaded areas indicate odd marine oxygen isotope stages.

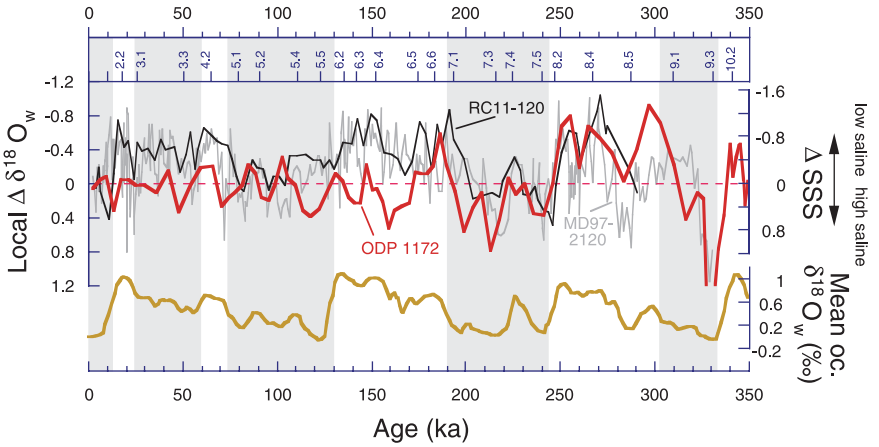

Figure 7. Comparison of local $\delta^{18}O_{seawater}$ and salinity anomalies (both expressed as deviation from the mean late Holocene (0–6 ka) value; $\Delta\delta^{18}O_{seawater}$ and ΔSSS) for the subantarctic Indian Ocean (RC11-120, thin black line, basic data by *Mashiotta et al.* [1999]), for East Tasman Plateau (Site1172A, thick red line, this study), and for Chatham Rise (MD97-2120, thin gray line, *Pahnke et al.* [2003]). The local $\delta^{18}O_{seawater}$ anomaly ($\Delta\delta^{18}O_{seawater}$) was derived from the planktonic $\delta^{18}O$ and $SST_{Mg/Ca}$ after correcting the planktonic $\delta^{18}O$ for mean ocean $\delta^{18}O_{seawater}$ changes [*Waelbroeck et al.*, 2002] (bottom curve). The equivalent salinity anomaly (ΔSSS) was calculated using the modern $\delta^{18}O_{seawater}$ versus salinity relationship for high southern latitudes between 40°S and 50°S of G. A. Schmidt et al. (http://www.giss.nasa.gov/data/o18data/, 1999). For a better comparability of cores, the $SST_{Mg/Ca}$ and $\delta^{18}O$ records were recalculated at 3.5 kyr steps. Dashed line indicates the mean Holocene values for the local $\delta^{18}O_{seawater}$ and salinity, respectively. Shaded areas indicate odd marine oxygen isotope stages.

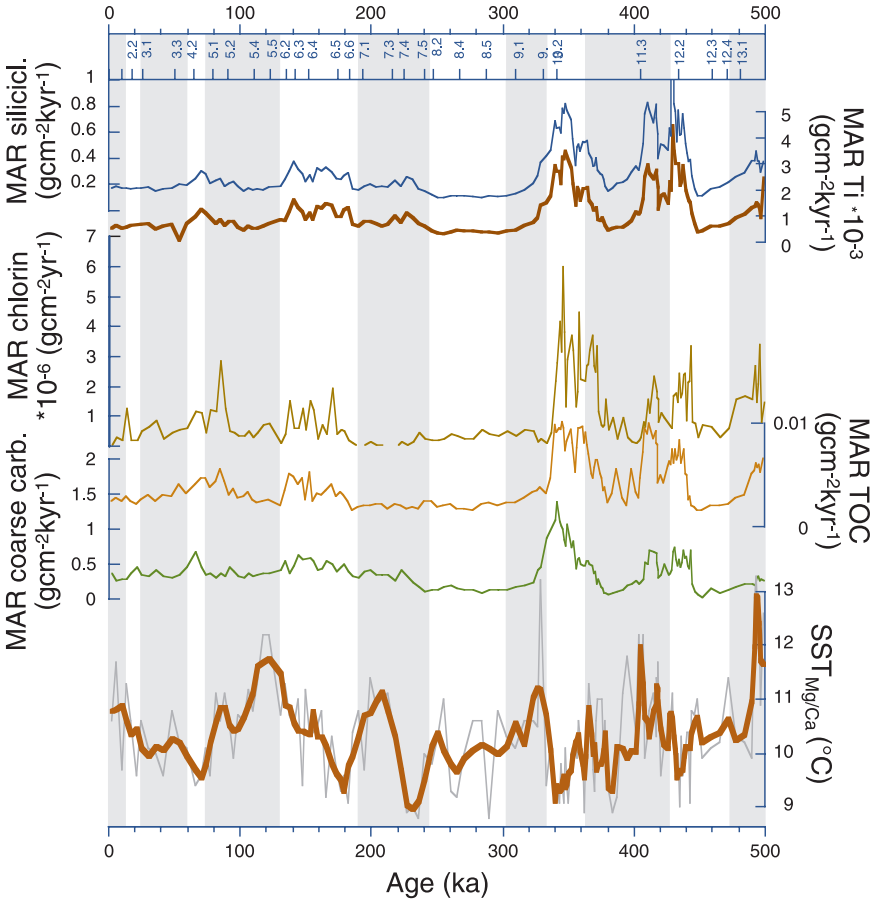

Figure 8. $SST_{Mg/Ca}$ variability over the past 500 kyr (*G. bulloides*) at Site 1172A (thick line: 7pt. smoothed, thin line: original data) in comparison to changes in marine productivity (assessed from accumulation rates of coarse (>63 μm) carbonate, total organic carbon (TOC), and chlorin) and terrigenous flux (inferred from titanium and siliciclastic concentrations normalized to unit variance) [*Nürnberg et al.*, 2004]. Shaded areas indicate odd marine oxygen isotope stages.

~120 ka, with decreased SSS during glacial MIS 6, 8, and 10. After 120 ka, the SSS record is attenuated with less pronounced, but still visible variability. The temporal variations in SSS at Chatham Rise [*Pahnke et al.*, 2003] resemble those in the subantarctic Indian Ocean (calculated from planktonic $\delta^{18}O$ and $SST_{Mg/Ca}$ of *Mashiotta et al.* [1999]), with similar amplitudes, and lowered SSS during glacial intervals. The SSS record of Site 1172A mirrors the salinity variations at Chatham Rise and within the subantarctic Indian Ocean from MIS 10 to 6, but shifts to conditions more similar to today afterward.

3.5. Spatial and Temporal Variability of the Subtropical Convergence

[25] Site 1172A on East Tasman Plateau is at the ideal location to monitor the position of the STC, as its core is located at ~45°S in the Tasman Sea [*Edwards and Emery*, 1982; *Belkin and Gordon*, 1996; *Rintoul et al.*, 1997]. We presuppose that spatial and temporal variations in the STC separating less saline (~34.5 [*Butler et al.*, 1992]), nutrient-rich Subantarctic Surface Water from oligotrophic, warm, and saltier (35.8 [*Butler et al.*, 1992]) Subtropical Surface Water are leaving clear signatures in marine productivity, SST and SSS over East Tasman Plateau. The attempt to combine reconstructions of SST and SSS (this study) with reconstructions of marine productivity and terrigenous flux [*Nürnberg et al.*, 2004] may help to further constrain both the paleo-position of the STC close to Tasmania and temporal and spatial variations in the East Australian Current system (Figure 8).

[26] When comparing the $SST_{Mg/Ca}$ record with changes in marine productivity (reflected in accumulation rates of coarse (>63 μm) carbonate, total

organic carbon and chlorin), and terrigenous flux (reflected in accumulation rates of siliciclastics and titanium) [*Nürnberg et al.*, 2004], a consistent pattern becomes apparent (Figure 8). In general, glacial $SST_{Mg/Ca}$ and SSS were lowered, and both marine productivity and eolian flux were enhanced. Such a scenario was clearly established during glacial MIS 12, MIS 10, and to a lesser degree during MIS 6. The extension of the Antarctic ice sheet and sea ice might have caused the displacement of the Southern Ocean oceanographic frontal systems to the north. The relative increase of marine productivity at low $SST_{Mg/Ca}$ at Site 1172A implies the northward movement of nutrient-rich but cool Subantarctic Surface Water across East Tasman Plateau, the northward retreat of the East Australian Current, and hence a shift of the STC to <44°S (in accordance with *Nees* [1997]). At these times, the Tasman Front, marking a coherent, meandering, zonal jet being related to the variability of the East Australian Current system [*Stanton*, 1981], moved northward to at least 32°S [*Martinez*, 1994b; *Nees*, 1997] implying an extended northward influence of Subantarctic waters into the Tasman Sea. Contemporaneously, the West Wind Drift belt, centered between the STC and the Antarctic Convergence (=Antarctic Polar Front), strengthened during glacial times and established an intensified anticyclonic wind gyre over Australia [*Kolla and Biscaye*, 1977; *Thiede*, 1979].

[27] During interglacials, predominantly high $SST_{Mg/Ca}$ and SSS and relatively low marine productivity and terrigenous flux [*Nürnberg et al.*, 2004] (Figure 8) imply that the STC separating cool, high-nutrient Subantarctic Surface Water from warm, saline, oligotrophic Subtropical Surface Water and hence the band of zonal westerlies responsible for the eolian dust flux were located south of East Tasman Plateau [*Nürnberg et al.*, 2004], and even south of South Tasman Rise [*Wells and Cornell*, 1997]. The warm East Australian Current was well established and propagated far south.

3.6. Latitudinal Spread of the STC Over East Tasman Plateau

[28] As described above, the temporal variations in $SST_{Mg/Ca}$ and SSS seen at Site 1172A are most likely caused by the changing position of the STC across that site. The northward migration of Subantarctic Surface Water causes freshening and cooling at the core location, while the southward migration of the STC during warm periods brings warm and high-saline Subtropical Surface Water. The degree of latitudinal spread of the STC through time, however, is still a matter of debate. *Nürnberg et al.* [2004] suggested that during interglacial times, the position of the STC mainly remained south of Tasman Rise, while during glacials, the STC moved north toward East Tasman Plateau, thus leading to an overall maximum latitudinal range of ~4° in the Tasman region. On the basis of a site further to the east, *Sikes et al.* [2002] proposed that the STC remained fixed over the Chatham Rise during the Last Glacial Maximum, with an associated strong thermal gradient across the rise [*Weaver et al.*, 1998].

[29] Here, we attempt to assess the latitudinal spread of the STC across Site 1172A from reconstructed $SST_{Mg/Ca}$ and SSS and compare it to the Subantarctic Indian Ocean and Chatham Rise regions. In Figure 9, the paleo-$SST_{Mg/Ca}$ versus paleo-SSS anomalies (mean values for glacial and interglacial MIS; stage definition according to *Martinson et al.* [1987] and *Bassinot et al.* [1994]) were plotted on top of the modern SST versus SSS values from a N-S-trending transect across Site 1772 (starting at 38.5°S and terminating at 53.5°S). Anomalies were calculated as deviations from the mean Holocene (0–6 ka) $SST_{Mg/Ca}$ and SSS-values, and centered at the modern SST and SSS conditions of the respective core locations.

[30] For the East Tasman Plateau Site 1172A, which is located at the northern boundary of the STC, the averaged interglacial and glacial paleo-$SST_{Mg/Ca}$ versus paleo-SSS anomalies predominantly plot into the modern SST versus SSS fields, defined by annual SST and SSS from 0–100 m (Figure 9). Standard deviations of paleo-SSS estimates, however, trespass the modern SST versus SSS field, most likely due to uncertainties in the SSS reconstruction. The averaged MIS 1 and MIS 5 $SST_{Mg/Ca}$ versus SSS anomalies are closest to the modern SST and SSS conditions at that site. Interglacial MIS 7, 9, and 11 exhibit consistently cooler $SST_{Mg/Ca}$. Glacial MIS 2–4, 6, 8, and 10 are rather similar in $SST_{Mg/Ca}$, while MIS 8 is less saline. All MIS scenarios agree with modern SST and SSS conditions being found 1–2° south of the present 1172A site location. The overall glacial/interglacial $SST_{Mg/Ca}$ amplitude is attenuated and implies that the position of the STC in relation to core 1172A did not change significantly over time. Site 1172A largely remained under quasi-constant thermal conditions. In spite of the minor SST and

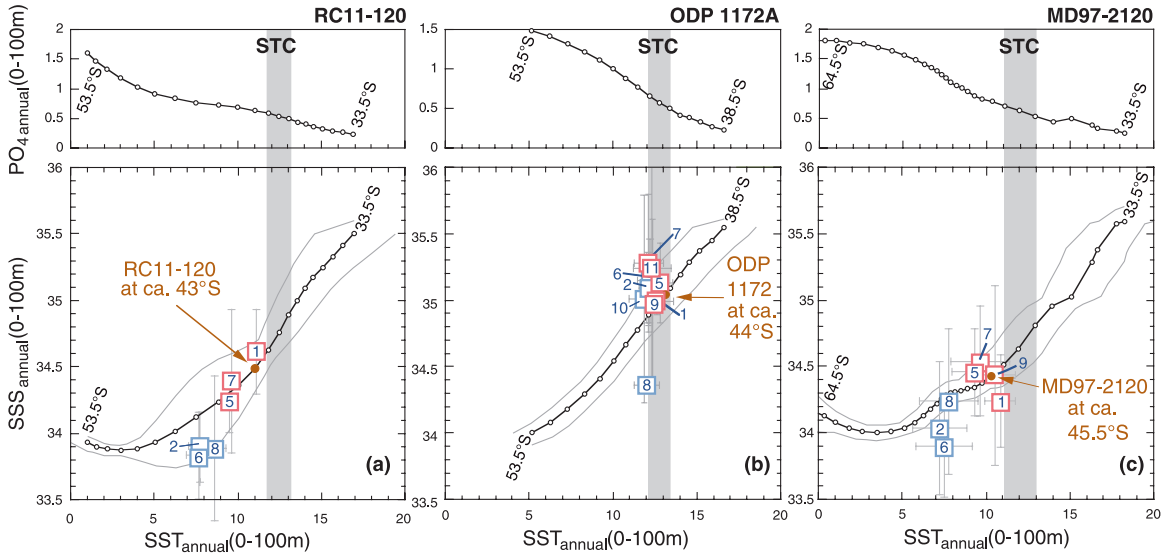

Figure 9. Paleo-$SST_{Mg/Ca}$ versus paleo-SSS anomalies in comparison to modern SST_{annual} versus SSS data from 0–100 m water depth for (a) subantarctic Indian Ocean core RC11-120, (b) East Tasman Plateau ODP Site 1172A, and (c) Chatham Rise core MD97-2120. Modern SST and SSS data are from north-south trending oceanographic profiles across the respective core locations (black line, where open circles denote 1° latitudinal steps; start and end points of transects are indicated; gray lines indicate standard deviations; data from *Levitus and Boyer* [1994]). Paleo-$SST_{Mg/Ca}$ versus paleo-SSS anomalies were calculated as deviations from the mean Holocene (0–6 ka) $SST_{Mg/Ca}$ and SSS-values, and centered at the modern SST and SSS conditions of the respective core locations (large red dots). Squares with numbers denote average glacial (MIS 2 [= MIS 2–4], 6, 8, 10) and interglacial (MIS 1, 5, 7, 9, 11) paleo-$SST_{Mg/Ca}$ versus paleo-SSS anomalies. Error bars indicate standard deviations derived from the entire range of glacial and interglacial SST and SSS values, respectively. Hatched areas mark the modern position of the STC, which is most likely defined by a drastic drop in SST and a subtle change in phosphate concentrations (uppermost diagram). Note: X and Y axes refer to absolute modern SST and SSS. Squares denote paleo-$SST_{Mg/Ca}$ and SSS anomalies and imply relative deviations from modern conditions.

SSS change at Site 1172A, the clearly enhanced marine productivity and terrigenous flux particularly during glacial MIS 12, 10, and 6, nevertheless, point to the increasing influence of Subantarctic Surface Water over East Tasman Plateau.

[31] The subantarctic Indian Ocean core RC11-120, located slightly south of the STC, is different. The averaged interglacial and glacial paleo-$SST_{Mg/Ca}$ versus paleo-SSS anomalies again plot into the modern SST versus SSS field. The maximum glacial/interglacial $SST_{Mg/Ca}$ range, however, is much larger than for Site 1172A (~3.5°C), while the SSS range is ~0.8 units (Figure 9). The averaged MIS 1 $SST_{Mg/Ca}$ versus SSS anomaly is close to the modern SST and SST conditions. Interglacial MIS 5 and 7 exhibit consistently cooler SST and lower SSS than MIS 1, resembling modern conditions being found ~1–1.5° further south of the RC11-120 core location. They are still warmer and higher saline than the glacial MIS. MIS 2–4 and MIS 6 are rather similar, while MIS 8 is warmer by ~1°C at comparable SSS. Glacial MIS reflect conditions corresponding to those existing today ~3° south of the core location.

[32] A similar pattern as seen in the Subantarctic Indian Ocean is visible at Chatham Rise core MD97-2120 located slightly south of the present-day STC. Averaged interglacial $SST_{Mg/Ca}$ and SSS conditions plot close to the modern SST and SSS conditions, while the glacial conditions are significantly cooler and lower saline, corresponding to modern values appearing ~6–8° south of the core location (Figure 9). The overall glacial/interglacial $SST_{Mg/Ca}$ amplitude is comparable to the Subantarctic Indian Ocean core, and amounts to ~4°C.

[33] It is interesting to note that at Chatham Rise and at the Subantarctic Indian Ocean core, interglacial MIS 1 is warmest and close to modern conditions, followed by MIS 7 and MIS 5, when considering averaged $SST_{Mg/Ca}$. Assuming that the hydrographical front and spacing of isotherms across fronts during past interglacials was similar to today, we speculate that the STC shifted further northward during MIS 7 and 5 by maximum 2°. For glacials,

it is most likely that isotherm spacing narrowed, and hence we are unable to quantify frontal movement. Nevertheless, since the pattern of sea surface cooling during glacials with lowest averaged $SST_{Mg/Ca}$ during MIS 2–4 and 6, and slightly warmer averaged $SST_{Mg/Ca}$ during MIS 8 is identical at both locations, we suspect that latitudinal shifts of the STC occurred synchronously in the subantarctic Indian Ocean and at Chatham Rise. The attenuated $SST_{Mg/Ca}$ and SSS signal, and accordingly, the relatively small hydrographic changes observed at East Tasman Plateau, however, are presumably related to the continuous influence of the warm East Australian Current in that area even during glacial times, buffering large-scale latitudinal variations of the STC.

4. Conclusions

[34] Combined measurements of Mg/Ca ratios and $\delta^{18}O$ values in tests of the planktonic foraminifer *G. bulloides* from ODP Site 1172A from East Tasman Plateau allowed us to reconstruct the surface ocean hydrography in the southwestern Tasman Sea over the last ~500,000 years. The core-top $SST_{Mg/Ca}$ estimate of 10.6–11.7°C corresponds to the modern austral spring water temperature at Site 1172A and suggests that *G. bulloides* records austral spring SST conditions in the Tasman Sea. The downcore $SST_{Mg/Ca}$ record comprises four major glacial-interglacial changes, showing high temperatures during warm periods and low temperatures during cool periods with an overall temperature range of ~5°C, from 9°C to 14°C. At terminations, the glacial/interglacial amplitude is ~2–3°C.

[35] The parallel analysis of $\delta^{18}O$ and Mg/Ca in the same biotic carrier allowed us to extract the $\delta^{18}O_{seawater}$ signal, which ranges between −0.2 and +2‰ at Site 1172A. The resulting SSS record shows pronounced and high-amplitude glacial/interglacial changes before ~120 ka, with lowered SSS during glacial MIS 6, 8, and 10. After 120 ka, the SSS record is attenuated with less pronounced, but still recognizable climatic variability.

[36] The commonly high $SST_{Mg/Ca}$ and SSS during interglacials correspond to intervals of low marine productivity and low terrigenous flux, implying that the STC separating cool, high-nutrient Subantarctic Surface Water from warm, saline, oligotrophic Subtropical Surface Water and hence the band of zonal westerlies responsible for the eolian dust flux were located south of East Tasman Plateau. The warm East Australian Current was well established during warm periods and propagated far south. Instead, $SST_{Mg/Ca}$ and SSS were lowered during glacials, while both marine productivity and eolian flux increased. Such surface ocean conditions dominated during glacial MIS 12, MIS 10, and to a lesser degree during MIS 6, and implied the displacement of the Southern Ocean oceanographic frontal systems to the north mainly due to the extension of the Antarctic ice sheet and sea ice.

[37] The comparison of our $SST_{Mg/Ca}$ and SSS records to those from comparable latitudes to the east (Chatham Rise) and to the west (subantarctic Indian Ocean) of Site 1172 revealed that the overall climatic signal at Site 1172A is largely attenuated. Nevertheless, the combination of enhanced marine productivity and terrigenous flux at times of lowered $SST_{Mg/Ca}$ and SSS, particularly during glacial MIS 12, 10, and 6, point to the growing influence of Subantarctic Surface Water at the East Tasman Plateau in line with the northward migration of the STC. During interglacials, instead, lowered marine productivity and terrigenous flux at higher $SST_{Mg/Ca}$ and SSS favor the presence of Subtropical Surface Water and the dominating impact of the East Australian Current at East Tasman Plateau. Frontal migrations appear to have been more pronounced in the subantarctic Indian Ocean and at Chatham Rise. $SST_{Mg/Ca}$ records, which show a much higher amplitude variability, exhibit a consistent pattern at both locations with lowest $SST_{Mg/Ca}$ during glacial MIS 2–4 and 6, and slightly warmer $SST_{Mg/Ca}$ during MIS 8. We suspect that latitudinal shifts of the STC occurred synchronously in the subantarctic Indian Ocean and at Chatham Rise, but were largely damped at East Tasman Plateau.

Acknowledgments

[38] This study used samples and data provided by the Ocean Drilling Program, which is sponsored by the U.S. National Science Foundation (NSF) and participating countries under the management of the Joint Oceanographic Institution (JOI) Incorporated. Funding of this research was provided by the German Science Foundation (DFG) within the authors' project Nu 60/7. We thank Neville Exon, James Kennett, and the Leg 189 Shipboard Scientific Party for their kind support. Critical comments from two anonymous reviewers, which improved the manuscript, are acknowledged. Further, we are grateful for valuable comments of J. Schönfeld, A. Sturm, and M. Regenberg. Technical support was kindly provided by S. Koch.

References

Almond, D., B. McGowran, and Q. Y. Li (1993), Late Quaternary foraminiferal record from the Great Australian Bight and its environmental significance, *Mem. Assoc. Australas. Paleontol.*, *15*, 417–428.

Armand, L. K. (1997), The use of diatom transfer functions in estimating sea-surface temperature and sea-ice in cores from SE-Indian ocean, Ph.D. thesis, 370 pp., Dept. of Geol., Aust. Natl. Univ., Canberra, Australia.

Bard, E., B. Hamelin, M. Arnold, L. Montaggioni, G. Cabioch, G. Faure, and F. Rougerie (1996), Sea level record from Tahiti corals and the timing of deglacial meltwater discharge, *Nature*, *382*, 241–244.

Barker, S., M. Greaves, and H. Elderfield (2003), A study of cleaning procedures used for foraminiferal Mg/Ca paleothermometry, *Geochem. Geophys. Geosyst.*, *4*(9), 8407, doi:10.1029/2003GC000559.

Bassinot, F. C., L. D. Labeyrie, E. Vincent, X. Quidelleur, N. J. Shackleton, and Y. Lancelot (1994), The astronomical theory of climate and the age of the Brunhes-Matuyama magnetic reversal, *Earth Planet. Sci. Lett.*, *126*, 91–108.

Belkin, I. M., and A. L. Gordon (1996), Southern Ocean fronts from the Greenwich meridian to Tasmania, *J. Geophys. Res.*, *101*, 3675–3696.

Berger, W. H. (1989), Global maps of ocean productivity, in *Productivity in the Ocean: Present and Past*, *Dahlem Workshop Rep. LS44*, edited by W. Berger et al., pp. 429–456, John Wiley, Hoboken, N. J.

Blunier, T., and E. J. Brook (2001), Timing of millennial-scale climate change in Antarctica and Greenland during the last glacial period, *Science*, *291*, 109–112.

Boyle, E. A. (1983), Manganese carbonate overgrowths on foraminifera tests, *Geochim. Cosmochim. Acta*, *47*, 1815–1819.

Broecker, W. S. (1989), The salinity contrast between the Atlantic and Pacific oceans during glacial times, *Paleoceanography*, *4*, 207–212.

Butler, E. C. V., J. A. Butt, E. J. Lindstrom, and P. C. Tildesley (1992), Oceanography of the Subtropical Convergence Zone around southern New Zealand, *N. Z. J. Mar. Freshwater Res.*, *26*, 131–154.

Caillon, N., J. P. Severinghaus, J. Jouzel, J. M. Barnola, J. Kang, and V. Y. Lipenkov (2003), Timing of atmospheric CO_2 and Antarctic temperature changes across Termination III, *Science*, *299*, 1728–1731.

Climate: Long-Range Investigation, Mapping, and Prediction (CLIMAP) (1981), Seasonal reconstructions of Earth's surface at the Last Glacial Maximum, *GSA Map Chart Ser., MC-36*, Geol. Soc. of Am., Boulder, Colo.

Cox, M. D. (1989), An idealized model of the world ocean, part I: The global scale water masses, *J. Phys. Oceanogr.*, *19*, 1730–1752.

Cresswell, G. (1987), The East Australian Current, report, *CSIRO Mar. Lab. Inf. Sheet 3*, Hobart, Tasmania, Australia.

Dekens, P. S., D. W. Lea, D. K. Pak, and H. J. Spero (2002), Core top calibration of Mg/Ca in tropical foraminifera: Refining paleotemperature estimation, *Geochem. Geophys. Geosyst.*, *3*(4), 1022, doi:10.1029/2001GC000200.

Edwards, R. J., and W. J. Emery (1982), Australasian Southern Ocean frontal structure during summer 1976–77, *Australas. J. Mar. Freshwater Res.*, *33*, 3–22.

Elderfield, H., and G. Ganssen (2000), Past temperature and delta-18O of surface ocean waters inferred from foraminiferal Mg/Ca ratios, *Nature*, *405*, 442–445.

Epstein, S., R. Buchsbaum, H. A. Lowenstamm, and H. C. Urey (1953), Revised carbonate-water isotopic temperature scale, *Geol. Soc. Am. Bull.*, *64*, 1315–1325.

Exon, N., et al. (2001), *Proceedings of the Ocean Drilling Program, Initial Reports* [online], vol. 189, edited by N. F. Exon, J. P. Kennett, and M. J. Malone, Ocean Drill. Program, College Station, Tex. (Available at http://www-odp.tami.edu/publications/189_IR/189ir.htm)

Fairbanks, R. G. (1989), A 17,000-year glacio-eustatic sea level record; influence of glacial melting rates on the Younger Dryas event and deep-ocean circulation, *Nature*, *342*(6250), 637–642.

François, R., M. P. Bacon, M. A. Altabet, and L. D. Labeyrie (1993), Glacial/interglacial changes in sediment rain rate in the SW Indian sector of subantarctic waters as recorded by ^{230}Th, ^{231}Pa, U, and δ^{15}N, *Paleoceanography*, *8*(5), 611–630.

Garner, D. M. (1959), The Subtropical Convergence in New Zealand waters, *Australas. J. Mar. Freshwater Res.*, *2*, 315–337.

Giraudeau, J. (1993), Planktonic foraminiferal assemblages in the surface sediments from the southwest African continental margin, *Mar. Geol.*, *110*, 47–62.

Guilderson, T. P., L. Burckle, S. Hemming, and W. R. Peltier (2000), Late Pleistocene sea level variations derived from the Argentine Shelf, *Geochem. Geophys. Geosyst.*, *1*(12), doi:10.1029/2000GC000098.

Hanebuth, T., K. Stattegger, and P. M. Grootes (2000), Rapid flooding of the Sunda Shelf: A late-glacial sea-level record, *Science*, *288*, 1033–1035.

Harle, K. J. (1997), Late Quaternary vegetation and climate change in southeastern Australia: Palynological evidence from marine core E55-6, *Palaeogeogr. Palaeoclimatol. Palaeoecol.*, *131*, 465–483.

Hays, J. D., J. A. Lozano, N. J. Shackleton, and G. Irving (1976), Reconstruction of the Atlantic and western Indian Ocean sectors of the 18,000 B. P. Antarctic Ocean , in *Investigation of Southern Ocean Paleoceanography and Paleoclimatology*, edited by R. M. Cline and J. D. Hays, *Mem. Geol. Soc. Am.*, *145*, 337–374.

Hemleben, C., and M. Spindler (1983), Recent advances in research on living planktonic foraminifera, in *Reconstruction of Marine Paleoenvironments*, *Micropaleontol. Bull. 30*, edited by J. E. Meulenkamp, pp. 141–170, State Univ. of Utrecht, Utrecht, Netherlands.

Hemleben, C., M. Spindler, and O. R. Anderson (1989), *Modern Planktonic Foraminifera*, 363 pp., Springer, New York.

Howard, W. R., and W. L. Prell (1992), Late Quaternary surface circulation of the Southern Indian Ocean and its relationship to orbital variations, *Paleoceanography*, *7*(1), 79–117.

Hut, G. (1987), Stable isotope reference samples for geochemical and hydrological investigations, Report to the Director General, 42 pp., Int. At. Energy Agency, Vienna.

Imbrie, J., J. D. Hays, D. G. Martinson, A. McIntyre, J. J. Morley, N. G. Pisias, W. L. Prell, and N. J. Shackleton (1984), The orbital theory of Pleistocene climate: Support from a revised chronology of the marine δ^{18}O record, in *Milankovitch and Climate, Part I*, *NATO ASI Ser., Ser. C*, *126*, 269–305.

Jouzel, J., G. Hoffmann, F. Parrenin, and C. Waelbroeck (2002), Atmospheric oxygen 18 and sea-level changes, *Quat. Sci. Rev.*, *21*, 307–314.

Kennett, J. P. (1977), Cenozoic evolution of Antarctic glaciation, the Circum-Antarctic Ocean, and their impact on global paleoceanography, *J. Geophys. Res.*, *82*, 3843–3959.

Kershaw, P., P. G. Quilty, B. David, S. Van Huet, and A. McMinn (2000), Paleobiogeography of the Quaternary of Australasia, *Mem. Assoc. Australas. Paleontol.*, *23*, 471–516.

King, A. L., and W. R. Howard (2003), Planktonic foraminiferal flux seasonality in Subantarctic sediment traps: A test for paleoclimate reconstructions, *Paleoceanography*, *18*(1), 1019, doi:10.1029/2002PA000839.

Kolla, V., and P. E. Biscaye (1977), Distribution and origin of quartz in the sediment of the Indian Ocean, *J. Petrol.*, *47*, 642–649.

Labeyrie, L. D., J. C. Duplessy, and P. L. Blanc (1987), Variations in mode off formation and temperature of oceanic deep waters over the past 125,000 years, *Nature*, *327*, 477–482.

Labracherie, M., L. D. Labeyrie, J. Duprat, E. Bard, M. Arnold, J.-J. Pichon, and J.-C. Duplessy (1989), The last deglaciation in the Southern Ocean, *Paleoceanography*, *4*, 629–638.

Lea, D., D. K. Pak, and H. W. Spero (2000), Climate impact of Later Quaternary equatorial Pacific sea surface temperature variations, *Science*, *289*, 1719–1724.

Levitus, S., and T. Boyer (1994), *World Ocean Atlas 1994*, vol. 4, *Temperature*, *NOAA Atlas NESDIS 4*, Natl. Oceanic and Atmos. Admin., Silver Spring, Md.

Martinez, J. I. (1994a), Late Pleistocene palaeoceanography of the Tasman Sea: Implications for the dynamics of the warm pool in the western Pacific, *Palaeogeogr. Palaeoclimatol. Palaeoecol.*, *112*, 19–62.

Martinez, J. I. (1994b), Late Pleistocene carbonate dissolution patterns in the Tasman Sea, in *Evolution of the Tasman Sea Basin*, edited by G. J. van der Lingen et al., pp. 215–228, A. A. Balkema, Brookfield, Vt.

Martinson, D. G., N. G. Pisias, J. D. Hays, J. Imbrie, T. C. More Jr., and N. J. Shackleton (1987), Age dating and the orbital theory of the ice ages: Development of a high-resolution 0 to 300,000-year chronostratigraphy, *Quat. Res.*, *27*, 1–29.

Mashiotta, T. A., D. W. Lea, and H. J. Spero (1999), Glacial-interglacial changes in Subantarctic sea surface temperature and δ^{18}O-water using foraminiferal Mg, *Earth Planet. Sci. Lett.*, *170*, 417–432.

Morley, J. J. (1989), Variations in high-latitudes oceanographic fronts in the southern Indian ocean: An estimation based on faunal changes, *Paleoceanography*, *4*, 547–554.

Morley, J. J., and J. D. Hays (1979), Comparison of glacial and interglacial oceanographic conditions in the South Atlantic from variations in calcium carbonate and radiolarian distributions, *Quat. Res.*, *12*, 396–408.

Morley, J. J., W. L. Prell, and W. R. Howard (1988), Response of the Southern Ocean over the Milankovitch frequency band, *Eos Trans. AGU*, *69*, 299.

Nanson, G. C., D. M. Price, and S. A. Short (1992), Wetting and drying of Australia over the past 300 ka, *Geology*, *20*, 791–794.

Nees, S. (1997), Late Quaternary paleoceanography of the Tasman Sea: The benthic foraminiferal view, *Palaeogeogr. Palaeoclimatol. Palaeoecol.*, *131*, 365–389.

Nees, S., L. Armand, P. DeDeckker, M. Labracherie, and V. Passlow (1999), A diatom and benthic foraminiferal record from the South Tasman Rise (southeastern Indian Ocean): Implications for paleoceanographic changes for the last 200,000 years, *Mar. Micropaleontol.*, *38*, 69–89.

Niebler, S. (1995), Rekonstruktionen von Paläo-Umweltparametern anhand von stabilen Isotopen und Faunenvergesellschaftungen planktischer Foraminiferen im Südatlantik, Ph.D. thesis, 220 pp., Univ. of Bremen, Bremen, Germany.

Nürnberg, D. (2000), Taking the temperature of past ocean surfaces, *Science*, *289*, 1698–1699.

Nürnberg, C. C., G. Bohrmann, M. Schlüter, and M. Frank (1997), Barium accumulation in the Atlantic sector of the Southern Ocean: Results from 190,000-year records, *Paleoceanography*, *12*(4), 594–603.

Nürnberg, D., A. Müller, and R. Schneider (2000), Paleo-sea surface temperature calculations in the equatorial east Atlantic from Mg/Ca ratios in planktic foraminifera: A comparison to sea surface temperature estimates from $U^{K'}_{37}$, oxygen isotopes, and foraminiferal transfer function, *Paleoceanography*, *15*(1), 124–134.

Nürnberg, D., N. Brughmans. J. Schönfeld, U. Ninnemann, and C. Dullo (2004), Paleo-export production, terrigenous flux and sea surface temperatures around Tasmania: Implications for glacial/interglacial changes in the Subtropical Convergence Zone, in *The Cenozoic Southern Ocean: Tectonics, Sedimentation, and Climate Change Between Australia and Antarctica*, *Geophys. Monogr. Ser.*, vol. 151, edited by N. Exon, J. P. Kennett, and M. Malone, pp. 291–317, AGU, Washington, D. C.

Okada, H., and P. Wells (1997), Late Quaternary nannofossil indicators of climate change in two deep-sea cores associated with the Leeuwin Current off Western Australia, *Palaeogeogr. Palaeoclimatol. Palaeoecol.*, *131*, 413–432.

Okuno, J., and M. Nakada (1999), Total volume and temporal variation of meltwater from last glacial maximum inferred from sea-level observations at Barbados and Tahiti, *Palaeogeogr. Palaeoclimat. Palaeoecol.*, *146*(1–4), 283–293.

Orsi, A. H., T. Whitworth III, and W. D. Nowlin (1995), On the meridional extent and fronts of the Antarctic Circumpolar Current, *Deep Sea Res., Part I*, *42*(5), 641–673.

Pahnke, K., R. Zahn, H. Elderfield, and M. Schulz (2003), 340,000-year centennial-scale marine record of Southern Hemisphere climatic oscillation, *Science*, *301*, 948–952.

Paillard, D., L. Labeyrie, and P. Yiou (1996), Macintosh program performs time-series analysis, *Eos Trans. AGU*, *77*, 379.

Passlow, V., W. Pixian, and A. R. Chivas (1997), Late Quaternary paleoceanography near Tasmania, southern Australia, *Palaeogeogr. Palaeoclimatol. Palaeoecol.*, *131*, 433–463.

Petit, J. R., et al. (1999), Climate and atmospheric history of the past 420,000 years from the Vostok Ice Core, Antarctica, *Nature*, *399*, 429–436.

Pichon, J. J., G. Bareille, M. Labracherie, L. D. Labeyrie, A. Baudrimont, and J. L. Turon (1992), Quantification of the biogenic silica dissolution in Southern Ocean sediments, *Palaeogeogr. Palaeoclimatol. Palaeoecol.*, *61*, 79–95.

Prell, W. L., W. H. Hutson, and D. F. Williams (1979), The Subtropical Convergence and late Quaternary circulation in the southern Indian Ocean, *Mar. Micropaleontol.*, *4*, 225–234.

Prell, W. L., J. Imbrie, D. G. Martinson, J. J. Morley, N. G. Pisias, N. J. Shackleton, and H. F. Streeter (1986), Graphic correlation of oxygen isotope stratigraphy application to the Late Quaternary, *Paleoceanography*, *1*, 137–162.

Rintoul, S. R., J. R. Donguy, and D. H. Roemich (1997), Seasonal evolution of the upper ocean thermal structure between Tasmania and Antarctica, *Deep Sea Res., Part I*, *44*, 1185–1202.

Roche, D., D. Paillard, A. Ganopolski, and G. Hoffmann (2004), Oceanic oxygen-18 at the present day and LGM: Equilibrium simulations with a coupled climate model of intermediate complexity, *Earth Planet. Sci. Lett.*, *218*, 317–330.

Rohling, E. J. (2000), Paleosalinity: Confidence limits and future applications, *Mar. Geol.*, *163*, 1–11.

Rohling, E. J., and G. R. Bigg (1998), Paleo-salinity and ^{18}O: A critical assessment, *J. Geophys. Res.*, *103*, 1307–1318.

Shackleton, N. J. (1974), Attainment of isotopic equilibrium between ocean water and the benthonic foraminifer genus *Uvigerina*: Isotopic changes in the ocean during the last glacial, in *Les Methodes Quantitative d'Etude des Variations*

du Climate au Cours du Pleistocene, edited by L. Labeyrie, *Colloq. Int. Cent. Natl. Rech. Sci.*, *219*, 203–210.

Shackleton, N. J. (1987), Oxygen isotopes, ice volume and sea level, *Quat. Sci. Rev.*, *6*, 183–190.

Shackleton, N. J., A. Berger, and W. R. Peltier (1990), An alternative astronomical calibration of the lower Pleistocene timescale based on ODP Site 677, *Trans. R. Soc. Edinburgh Earth Sci.*, *81*, 251–261.

Siddall, M., et al. (2003), Sea-level fluctuations during the last glacial cycle, *Nature*, *423*(6942), 853–858.

Sikes, E. L., W. R. Howard, H. L. Neil, and J. K. Volkman (2002), Glacial-interglacial sea surface temperature changes across the subtropical front east of New Zealand based on alkenone unsaturation ratios and foraminiferal assemblages, *Paleoceanography*, *17*(2), 1012, doi:10.1029/2001PA000640.

Stanton, B. R. (1981), An oceanographic survey of the Tasman Front, *N. Z. J. Mar. Freshwater Res.*, *15*, 289–297.

Stickley, C. E., et al. (2004), Late Cretaceous-Quaternary biomagnetostratigraphy of ODP Sites 1168, 1170, 1171 and 1172, Tasmanian Gateway, *Proc. Ocean Drill. Program Sci. Results*, *189*, 57 pp.

Sturm, A. (2004), Changes in ocean circulation and carbonate chemistry in the Australian sector of the Southern Ocean during the last 500,000 years, Ph.D. thesis, 114 pp., Univ. Kiel, Kiel, Germany.

Tchernia, P. (1980), *Descriptive Regional Oceanography*, Elsevier, New York.

Thiede, J. (1979), Wind regimes of the Late Quaternary southwest Pacific Ocean, *Geology*, *7*, 259–262.

Tiedemann, R., M. Sarnthein, and N. J. Shackleton (1994), Astronomic timescale for the Pliocene Atlantic $\delta^{18}O$ and dust flux records of Ocean Drilling Program Site 659, *Paleoceanography*, *9*, 619–638.

Uddstrom, M. J., and N. A. Oien (1999), On the use of high-resolution satellite data to describe the spatial and temporal variability of sea surface temperatures in the New Zealand region, *J. Geophys. Res.*, *104*(C9), 20,729–20,751.

Villanoy, C. L., and M. Tomczak (1991), Influence of Bass Strait Water on the Tasman Sea Thermocline, *Australas. J. Mar. Freshwater Res.*, *42*, 451–464.

Vogelsang, E. (1990), Paläo-Ozeanographie des Europäischen Nordmeeres an Hand stabiler Kohlenstoff- und Sauerstoffisotope, *Ber. Sonderforschungsbereich 313, Univ. Kiel*, *23*, pp. 1–136, Univ. Kiel, Kiel, Germany.

Waelbroeck, C., L. Labeyrie, E. Michel, J. C. Duplessy, J. F. McManus, K. Lambeck, E. Balbon, and M. Labracherie (2002), Sea-level and deep water temperature changes derived from benthic foraminifer isotopic records, *Quat. Sci. Rev.*, *21*, 295–305.

Wang, L., M. Sarnthein, J.-C. Duplessy, J.-C. Erlenkeuser, S. Jung, and U. Pflaumann (1995), Paleo sea surface salinities in the low-latitude Atlantic: The $\delta^{18}O$ record of *Globigerinoides ruber* (white), *Paleoceanography*, *10*(4), 749–761.

Weaver, P. P. E., L. Carter, and H. L. Neil (1998), Response of surface water masses and circulation to Late Quaternary climate change east of New Zealand, *Paleoceanography*, *13*(1), 70–83.

Wells, P. E., and R. Cornell (1997), Movement of hydrological fronts and widespread erosional events in the southwestern Tasman Sea during the Late Quaternary, *Aust. J. Earth Sci.*, *44*, 105–112.

Wells, P., and H. Okada (1997), Response of nannoplankton to major changes in sea-surface temperature and movements of hydrological fronts over DSDP Site 594 (south Chatham Rise, southeastern New Zealand), during the last 130 kyr, *Mar. Micropaleontol.*, *32*, 341.

Williams, D. F. (1976), Late Quaternary fluctuations of the Polar Front and Subtropical Convergence in the Southeast Indian Ocean, *Mar. Micropaleontol.*, *1*, 363–375.